Nucleophilic Activation by Positioning in Phosphoryl Transfer Catalyzed by Nucleoside Diphosphate Kinase[†,‡]

Suzanne J. Admiraal,[§] Benoit Schneider,[∥] Philippe Meyer,[⊥] Joël Janin,[⊥] Michel Véron,[∥] Dominique Deville-Bonne,[∥] and Daniel Herschlag*[,§]

Department of Biochemistry, Beckman Center B400, Stanford University, Stanford, California 94305-5307, Unité de Régulation Enzymatique des Activités Cellulaires, CNRS URA 1773, Institut Pasteur, 25 rue du Dr. Roux, 75724 Paris Cedex 15, France, and the Laboratoire d'Enzymologie et Biochimie Structurales, CNRS UPR 9063, 91198 Gif-sur-Yvette, France

Received November 19, 1998; Revised Manuscript Received February 5, 1999

ABSTRACT: The nonenzymatic reaction of ATP with a nucleophile to generate ADP and a phosphorylated product proceeds via a dissociative transition state with little bond formation to the nucleophile. Consideration of the dissociative nature of the nonenzymatic transition state leads to the following question: To what extent can the nucleophile be activated in enzymatic phosphoryl transfer? We have addressed this question for the NDP kinase reaction. A mutant form of the enzyme lacking the nucleophilic histidine (H122G) can be chemically rescued for ATP attack by imidazole or other exogenous small nucleophiles. The ATP reaction is 50-fold faster with the wild-type enzyme, which has an imidazole nucleophile positioned for reaction by a covalent bond, than with H122G, which employs a noncovalently bound imidazole nucleophile [$(k_{cat}/K_M)^{ATP}$]. Further, a 4-fold advantage for imidazole positioned in the nucleophile binding pocket created by the mutation is suggested from comparison of the reaction of H122G and ATP with an imidazole versus a water nucleophile, after correction for the intrinsic reactivities of imidazole and water toward ATP in solution. X-ray structural analysis shows no detectable rearrangement of the residues surrounding His 122 upon mutation to Gly 122. The overall rate effect of $\sim 10^2$-fold for the covalent imidazole nucleophile relative to water is therefore attributed to positioning of the nucleophile with respect to the reactive phosphoryl group. This is underscored by the more deleterious effect of replacing ATP with ATPγS in the wild-type reaction than in the imidazole-rescued mutant reaction, as follows. For the wild-type, ATPγS presumably disrupts positioning between nucleophile and substrate, resulting in a large thio effect of 300-fold, whereas precise alignment is already disrupted in the mutant because there is no covalent bond to the nucleophile, resulting in a smaller thio effect of 10-fold. In summary, the results suggest a catalytic role for activation of the nucleophile by positioning in phosphoryl transfer catalyzed by NDP kinase.

Reaction of ATP with a nucleophile to produce ADP and a phosphorylated product is ubiquitous in biological chemistry. Enzymes that catalyze phosphoryl transfer include ATPases that use a water nucleophile to attack ATP, small molecule kinases that use metabolites as nucleophiles, and protein kinases that undergo nucleophilic reaction with ATP at amino acid side chains. In molecular detail, all of these enzymatic reactions reduce to the phosphoryl group transfer diagrammed in Scheme 1. A nucleophile, almost always an oxygen or nitrogen nucleophile, attacks ATP at the γ-phosphate. Products of the reaction are an ADP leaving group and a phosphorylated nucleophile. Clearly the nucleophile is important in determining the identity of the phosphorylated product. However, the catalytic importance of the nucleophile in this reaction class is less apparent.

Scheme 1

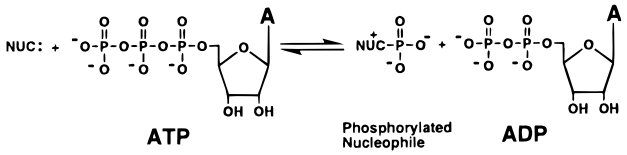

A large body of evidence supports the existence of a dissociative, metaphosphate-like transition state for nonenzymatic reactions of phosphate monoesters, acyl phosphates, phosphorylated amines, and phosphoanhydrides such as ATP (Figure 1). These data include near-zero entropies and volumes of activation, a large bridge ^{18}O effect, small Brønsted $\beta_{nucleophile}$ values, and large negative $\beta_{leaving\ group}$ values (*1*−*3*, *5*). Although it has been proposed that bound metal ions on enzymes may convert dissociative phosphoryl transfer into a more associative process, metal ion coordination to ATP and *p*-nitrophenyl phosphate has no effect on

[†] This work was supported by a Howard Hughes Medical Institute Junior Faculty Scholar Award to D.H. and by grants from the Agence Nationale de Recherche contre le SIDA (ANRS) to M.V. and J.J. S.J.A. is a Howard Hughes Medical Institute Predoctoral Fellow.

[‡] Atomic coordinates have been deposited at the Brookhaven Protein Data Bank under the file name 1B4S.

* To whom correspondence should be addressed. Phone: 650-723-9442. Fax: 650-723-6783. E-mail: herschla@cmgm.stanford.edu.

[§] Stanford University.

[∥] Institut Pasteur.

[⊥] Laboratoire d'Enzymologie et Biochimie Structurales.

10.1021/bi9827565 CCC: $18.00
Published on Web 03/25/1999

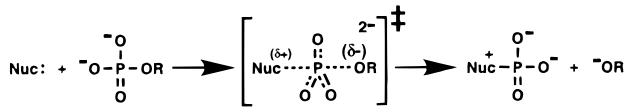

FIGURE 1: A dissociative transition state for phosphoryl transfer. The dissociative transition state has a small amount of bond formation to the incoming nucleophile and a large amount of bond cleavage to the outgoing leaving group. Bonds between phosphorus and the nonbridging phosphoryl oxygens of the transferred phosphoryl group are depicted as having a bond order greater than one [the actual nature of the bonding in metaphosphate and metaphosphate-like species is uncertain (*55*−*57*), so the two negative charges present in the transition state have not been assigned to particular atoms in the figure]. Associative transition states have a large amount of bond formation to the incoming nucleophile, a small amount of bond cleavage to the outgoing leaving group, and negative charge accumulation on the transferred phosphoryl group [ref *3*;, see also footnote 2]. "Phosphoryl transfer" generally refers to the transfer of PO_3^{2-}, $P(OR)O_2^-$, or $P(OR)_2O$ moieties. This paper addresses reactions of monosubstituted phosphoryl groups for which PO_3^{2-} is transferred; for simplicity, phosphoryl transfer is used to describe this subset of reactions in the text.

the transition state structures for reactions of these compounds (*5*, *6*). Investigations of nonenzymatic phosphoryl transfer further suggest that the energy surface in the vicinity of the transition state for these reactions is steep, making the transition state difficult to change (*6*−*8*). The simplest expectation for reaction of ATP and other phosphoryl donors at the active site of an enzyme is then that the reaction follows a dissociative, metaphosphate-like transition state similar to that observed in solution. Linear free-energy relationships (LFERs)[1] and ^{18}O isotope effects support dissociative transition states for the reactions of several phosphoryl transfer enzymes, as has been summarized elsewhere (*3*, *9*−*11*).

When there is little bond formation to the incoming nucleophile in a dissociative transition state, can enzymatic activation of the nucleophile contribute to catalysis? Conceptually, two types of activation can be envisioned, chemical activation and entropic, or positional, activation (*12*, *13*). Chemical activation entails stabilization of the nucleophile in the transition state, either by proton transfer to a general base catalyst or by electrostatic interactions with active site residues. General base catalysis and electrostatic stabilization of positive charge development on the nucleophile may provide substantial rate enhancement in an associative transition state. However, increased nucleophilicity due to chemical activation is not expected to confer a large rate advantage in a highly dissociative transition state, which has little bond formation to the nucleophile.[2]

Entropic activation describes the ability of an enzyme to align nucleophile and substrate with respect to one another, decreasing the entropic barrier that exists for the uncatalyzed reaction. Entropy is presumably lost upon even a small amount of bond formation, but the degree to which entropy loss scales with bond formation, as judged by LFERs, is not known. The amount of catalysis that may be derived from entropic activation of a nucleophile in a dissociative transition state is therefore also unknown, although large entropic advantages have previously been described for reactions that appear to proceed through associative transition states (*12*−*15*).

We have investigated nucleophilic activation in the NDPK reaction. This enzyme interconverts NTPs and NDPs by catalyzing successive phosphoryl transfers, first transferring a phosphoryl group from an NTP to histidine to form a phosphorylated enzyme and an NDP, and then catalyzing a second transfer between the phosphorylated enzyme and another NDP. NDPK was an attractive enzyme system for this study because it uses a histidine nucleophile. Phosphorylation of histidine (or other amines) gives a product that does not require deprotonation for stability at pH values near neutrality, whereas a proton must be lost in analogous reactions with oxygen nucleophiles in order to form a stable product (e.g., $HO-PO_3^{2-}$ instead of $H_2O^+-PO_3^{2-}$). In the absence of this requirement, nucleophilic activation by positioning may more readily be separated from nucleophilic activation by general base catalysis.

H122G, an NDPK mutant in which the nucleophilic histidine has been replaced by glycine, can be chemically rescued by exogenous Im and other small nucleophiles. This has allowed us to probe the catalytic advantage provided by a covalent linkage and a binding pocket for the nucleophile. The results suggest that entropic activation of the nucleophile contributes $\sim 10^2$-fold to catalysis.

EXPERIMENTAL PROCEDURES

Materials. Im was obtained from Baker, and amines and 4-methyl-5-imidazolemethanol were from Aldrich and were the highest purity available. Ultrapure ATP was from Pharmacia; ADP, GDP, and ATPγS were from Boehringer Mannheim. Unpurified [γ-^{32}P]ATP and [^{35}S]ATPγS were obtained from Amersham. Multiple radioactive bands were

[1] Abbreviations: LFER, linear free-energy relationship; NDPK, *Dictyostelium* nucleoside diphosphate kinase; ATPγS, adenosine-5′-*O*-(3-thiotriphosphate); Im, imidazole; ImP, imidazole phosphate; P_i, inorganic phosphate; k_{rel}, rate constant relative to analogous water reaction; PAGE, polyacrylamide gel electrophoresis; HPLC, high-performance liquid chromatography;.Tris-HCl, tris(hydroxymethyl)aminomethane hydrochloride; EPPS, 4-(2-hydroxyethyl)-1-piperazinepropanesulfonic acid; EDTA, ethylenediaminetetraacetic acid; MES, 4-morpholineethanesulfonic acid; MOPS, 4-morpholinepropanesulfonic acid; HEPES, 4-(2-hydroxyethyl)-1-piperazineethanesulfonic acid; CHES, 2-(cyclohexylamino)ethanesulfonic acid; CAPS, 3-cyclohexylamino-1-propanesulfonic acid.

[2] There is a continuum of possible transition states for phosphoryl transfer, ranging from a fully dissociative transition state, in which there is no bond formation to the nucleophile and essentially complete bond cleavage to the leaving group, to a fully associative transition state, in which there is complete bond formation to the nucleophile accompanied by development of a positive charge on the nucleophile and no significant bond cleavage to the leaving group (*1*−*3*). We adopt an operational definition of a dissociative transition state as one in which the sum of bonding between phosphorus and the incoming nucleophile and outgoing leaving group is less than one (i.e., bond order decreases in going from the ground state to the transition state), and an operational definition of an associative transition state as one in which the sum of bonding between phosphorus and the incoming nucleophile and outgoing leaving group is greater than one (i.e., bond order increases in going from the ground state to the transition state). Note that transition states that are only slightly dissociative or slightly associative are similar according to this definition and much more similar to each other than to either extreme. The data cited in the text suggest that the transition state for nonenzymatic phosphoryl transfer from ATP has a large amount of dissociative character. The degree to which chemical activation of the nucleophile can be catalytic depends on where along the continuum a transition state is located. General base catalysis or electrostatic interactions with developing charge on the nucleophile can stabilize even a dissociative transition state to the extent that there is bonding and therefore some charge build-up in the transition state.

Scheme 2

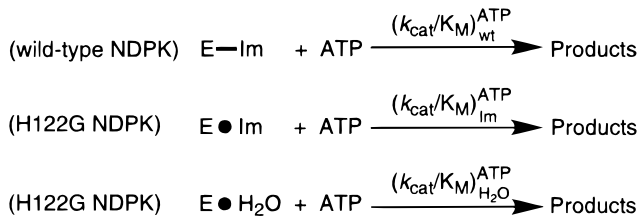

detected when radiolabeled nucleotides were analyzed by PAGE and exposed to film (Kodak), so the radiolabeled nucleotides were purified by elution with water from 15% nondenaturing polyacrylamide gels prior to use in experiments. Nitrocellulose membranes were from Schleicher and Schell. Water was doubly distilled from an all-glass apparatus.

Site-Directed Mutagenesis. Mutant H122G *Dictyostelium* NDPK was prepared by site-directed mutagenesis according to Kunkel (*16*), using the oligonucleotide 5′-GAAACAT-CATC*GGC*GGTTCTGATTC-3′. Altered bases as compared with the wild-type sequence are in italics. The mutation was verified by DNA sequencing.

Enzyme Purification. Wild-type and mutant *Dictyostelium* NDPKs were overexpressed in *Escherichia coli* (XL1-Blue) using plasmid *pndk* as described (*17*), with minor modifications. The cell extract was loaded at pH 8.4 onto a Q Sepharose matrix that retained only *E. coli* NDPK (*18*), and the flow-through was adsorbed on an Orange A matrix (Dyematrex, Amicon) at pH 7.5. After washing with Tris buffer, the enzyme was eluted by a NaCl gradient (0−1.5 M) in 50 mM Tris-HCl, pH 7.5. The protein was concentrated with an Amicon ultrafiltration cell, equilibrated in 50 mM Tris-HCl, pH 7.5, and stored at −20 °C. A 2−3-fold decrease in H122G activity was observed during storage of the enzyme over a one year period. Protein concentration was determined using the calculated extinction coefficient at 280 nm: 9200 M^{-1} cm^{-1} (*19*). Proteins were purified to homogeneity as judged by SDS−PAGE. Enzyme concentration was expressed as the concentration of 17 kDa subunits.

General Kinetic Methods for Reactions of ATP and H122G. H122G reactions were performed at 25 °C in buffered solutions of ionic strength 0.3 M (KCl) in the presence of 5 mM $MgCl_2$ and varying concentrations of Im and H122G (10−200 nM) to obtain $(k_{cat}/K_M)^{ATP}_{Im}$ (Scheme 2).

Reaction rates were linearly dependent on enzyme concentration. The rate of the H122G reaction with Im was pH-independent between pH 7 and 9 (see Figure 4B in Results), so a buffer composition of 50 mM potassium EPPS, pH 7.8, was routinely used. Im stocks were adjusted to the reaction pH with small amounts of KOH. Reactions were initiated by the addition of substrate ATP (100−500 nM) containing trace [γ-^{32}P]ATP, and aliquots were removed at specified times and quenched by the addition of an equal volume of 20 mM EDTA (pH 8) in 20% glycerol. Reaction rates were linearly dependent upon ATP concentration under these conditions, indicating that ATP was subsaturating. Radiolabeled substrate (ATP) and products (ImP and P_i) were separated by electrophoresis on 15% nondenaturing polyacrylamide gels, and their ratios at each time point were quantitated with a Molecular Dynamics PhosphorImager. Data analysis was performed using Kaleidagraph (Abelbeck Software), and exponential fits to the data typically gave $R \geq 0.99$. Analogous reactions were carried out without Im to follow the hydrolysis reaction [$(k_{cat}/K_M)^{ATP}_{H_2O}$; Scheme 2].

Inhibition of H122G Reactions by 4-Methyl-5-imidazolemethanol. Reactions of 50 nM H122G and 100 nM ATP in the presence or absence of 10 mM Im were performed as described above but with added 4-methyl-5-imidazolemethanol. For the hydrolysis reaction, the reaction velocity was linearly dependent upon ATP and H122G concentrations, indicating that the second-order reaction of ATP and H122G was followed. For the Im reaction, the reaction velocity was linearly dependent upon Im, ATP, and H122G, indicating that the third-order reaction of these components was followed.

pH Rate Profiles of H122G Reactions. Reactions of 50 nM H122G and 100 nM ATP in the presence or absence of 10 mM Im were performed as described above using the following buffers at 50 mM concentration: potassium MES, pH 5.6 and 6.1; potassium MOPS, pH 6.6 and 7.1; potassium HEPES, pH 7.3; potassium EPPS, pH 7.8; Tris-HCl, pH 8.6; potassium CHES, pH 8.8 and 9.3; and potassium CAPS, pH 9.9 and 10.5. As in the inhibition experiment described above, the second-order hydrolysis of ATP by H122G and the third-order reaction of ATP, Im, and H122G were followed.

General Kinetic Methods for Reactions of ATP and Wild-Type NDPK. Wild-type NDPK reactions were performed and analyzed similarly to H122G reactions, but different assays were required. As for H122G, wild-type reactions were performed at 25 °C in 50 mM potassium EPPS, pH 7.8, and ionic strength 0.3 M (KCl), with 5 mM $MgCl_2$. The wild-type reactions were carried out with 1 nM NDPK, 100 nM ATP with trace [γ-^{32}P]ATP, and 3 μM unlabeled GDP to obtain $(k_{cat}/K_M)^{ATP}_{wt}$ (Scheme 2). Reactions were initiated by the addition of ATP, and aliquots were removed at specified times and quenched by the addition of an equal volume of 20 mM EDTA, pH 8, in 20% glycerol. The radiolabeled ATP substrate and GTP product were separated by electrophoresis on 15% polyacrylamide gels and analyzed as described above. ATP donor, GDP acceptor, and wild-type NDPK concentrations were varied to ensure that the observed rate constant reported on the second-order reaction between ATP and wild-type NDPK and was independent of the concentration of GDP.

The value of $(k_{cat}/K_M)^{ATP}_{wt}$ obtained via this method was within 5-fold of previous measurements (*20*, *21*) and within 2-fold of a value obtained using an independent filter binding method to measure production of phosphoenzyme from radiolabeled ATP. For the filter binding experiments, reactions were carried out as above, but GDP acceptor was omitted, and aliquots were quenched by the addition of an excess of 20 mM EDTA in 10 mM NaOH. Nitrocellulose membranes were presoaked in the quench solution and placed on a Hoefer 10-well filter binding apparatus, and samples were applied to the membranes. Membranes were immediately washed with quench solution, dried, and placed in scintillation vials containing Econo-safe counting cocktail (Research Products International). The [γ-^{32}P]ATP that had been converted to ^{32}P-labeled phosphoenzyme was quantitated as radioactivity adhering to membranes by scintillation

counting. The concentrations of ATP and wild-type NDPK were varied to ensure that the observed rate constants reported the second-order reaction between the two components.

Inhibition of Wild-Type NDPK Reactions by Im. Reactions of wild-type NDPK and ATP were performed in the presence of acceptor GDP as described above but with added Im. Im stocks were adjusted to the reaction pH with small amounts of KOH.

Reactions of ATPγS and Definition of Thio Effect. Reactions of ATPγS with H122G and wild-type NDPK contained 1 mM dithiothreitol but were otherwise performed as described for reactions of ATP, with the substitution of ATPγS and trace [^{35}S]ATPγS for ATP and trace [γ-^{32}P]ATP; control experiments showed that dithiothreitol has no effect on reactions of ATP. Thio-substituted substrates and products were separated, and data were analyzed as described above for the unsubstituted compounds. The thio effect is defined as the ratio of the rate constant for reaction of the oxygen substrate relative to the sulfur substrate: $(k_{cat}/K_M)^{ATP}/(k_{cat}/K_M)^{ATP\gamma S}$.

Reactions of H122G with Amines. Reactions of H122G and ATP were performed at 25 °C in the presence of a series of amine nucleophiles. Typical reactions contained 1 μM H122G, 25−500 mM amine, 5 mM $MgCl_2$, and 100 nM ATP with trace [γ-^{32}P]ATP. Reaction pH was varied depending upon the pK_a of the amine in question: for reactions of amines with pK_a values less than 10, 25 mM potassium CAPS, pH 10.0, routinely served as buffer, whereas reactions of amines with pK_a values greater than 10 were self-buffered at pH values near their pK_a. In all reactions ionic strength was maintained at 0.3 M (KCl), and the actual concentration of the nucleophilic amine species ([RNH_2], as determined by amine pK_a and reaction pH) was used in calculations. At these high pH values, H122G was not maximally active (see Figure 4B in Results); however, this is not expected to affect the results because relative rate constants with respect to water (k_{rel}) rather than absolute rate constants were measured. As expected, the k_{rel} values were unaffected by changes in pH.

Reactions were carried out as described previously, with aliquots quenched by addition of an equal volume of 20 mM EDTA, pH 8. These aliquots were loaded onto an anion-exchange HPLC column (Dionex Nucleopac PA-100, 9 × 250 mm), and a LiCl gradient (0.01−1 M LiCl in 10% acetonitrile, 10 mM NaOH) was used to separate amine phosphate products from P_i and ATP. ^{32}P-Containing substrate and products were quantitated by scintillation counting. ATP and P_i peaks were identified by comparison to known standards. An additional radioactive peak that eluted prior to P_i and ATP appeared only in samples containing amine, and the amount formed was dependent on amine concentration; this peak was therefore identified as amine phosphate product. Amine phosphate products were only detected in reactions that contained H122G, and absolute rate constants for water and amine reactions were dependent on H122G concentration (although relative rate constants of amines with respect to water remained constant). The ratio of amine phosphate to P_i was constant throughout a particular time course, indicating that no secondary reactions involving the reaction products were occurring.

Scheme 3

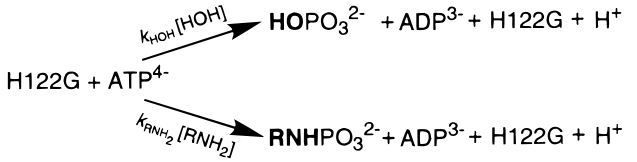

$$k_{rel} = \frac{k_{RNH_2}}{k_{HOH}} = \frac{\text{(fraction RNHPO}_3\text{)}}{[RNH_2]} \times \frac{[HOH]}{\text{(1 - fraction RNHPO}_3\text{)}}$$

The relative rate constant (k_{rel}) for the reaction of a given amine with respect to water was determined from the nucleophilic amine concentration of the original reaction ([RNH_2]) and the fraction of total product present as amine phosphate, according to the equation in Scheme 3. The same k_{rel} values, within error, were obtained for reactions performed at different amine concentrations. Each k_{rel} value in Table 3 represents an average of at least 3 separate HPLC runs; the average for several amines includes controls for different reaction pH, different reaction times, and different amine concentrations, as described above; k_{rel} values measured for individual amines varied over a range of ∼2-fold in different experiments.

Protein Crystallization and Structure Solution. The H122G protein was concentrated by ultrafiltration on Microcon-10 membranes (Amicon) and equilibrated in 20 mM $MgCl_2$, 50 mM Tris-HCl, pH 7.5. Crystallization occurred in a few days at 18 °C in hanging drops containing 21% PEG 400 (Merck), 20 mM $MgCl_2$, 100 mM Tris-HCl, pH 7.5, and 10 mM ATP (Sigma) over wells containing 42% PEG 400 in the same buffer without ATP. The crystals belong to trigonal space group $P3_121$ with cell parameters $a = b = 70.0$ Å and $c = 151.7$ Å, and have a trimer in the asymmetric unit.

X-ray diffraction data were collected at the D41 station of the LURE-DCI synchrotron radiation center (Orsay, France), using a single crystal that was flash-cooled in liquid nitrogen and kept at 100 K using an Oxford Cryosystem during data collection. The station was equipped with a MAR research image plate, and the wavelength was set to 1.375 Å. We recorded 72° of rotation at a rate of 1° per 4 min exposure and per image. Data processing was performed with DENZO (*22*) and data reduction with ScalePack. Further processing used the CCP4 program suite (*23*). Statistics are reported in Table 1.

The space group of the H122G crystals was the same as for the complex of wild-type *Dictyostelium* NDPK with Mg·ADP and AlF_3, and the cell parameters were similar (*24*). Thus, the orientation of the molecule was checked by molecular replacement using this complex as a search model. An electron density map calculated without the nucleotide clearly showed the absence of the His 122 side chain and the presence of a nucleotide at the active site of all three subunits in the asymmetric unit. The structure was refined using X-PLOR (*25*) under moderate noncrystallographic symmetry restraints. The final model has an *R* factor of 20.3% at 2.5 Å resolution (Table 1). The subunits are labeled A, B, and C.

RESULTS

Chemical Rescue of H122G by Im. To investigate nucleophilic activation in the NDPK reaction, we prepared the

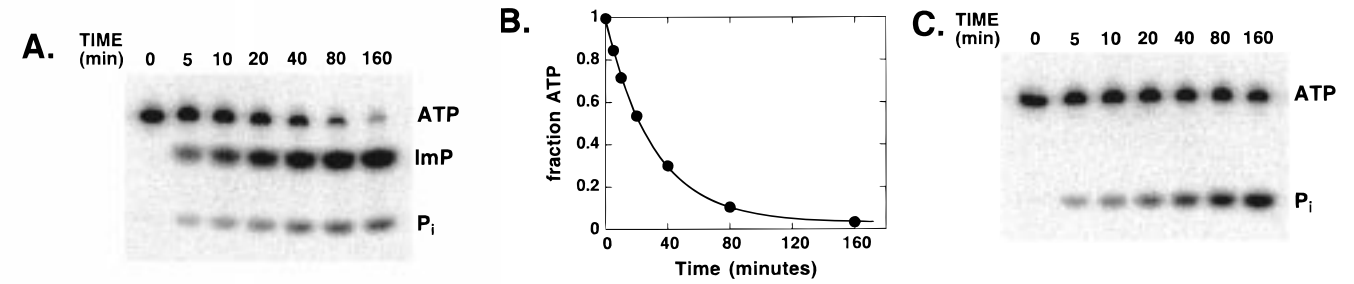

FIGURE 2: Chemical rescue of H122G. (A) PAGE analysis of the time course of the H122G-catalyzed reaction of ATP in the presence of 60 mM Im and 75 nM H122G. (B) Quantitation of the data in panel A. An exponential fit to the data gives $k_{obs} = 0.032$ min^{-1}. (C) PAGE analysis of the time course of the H122G-catalyzed hydrolysis of ATP in the absence of Im. An exponential fit to the data in panel C gives $k_{obs} = 0.0039$ min^{-1} (not shown).

Table 1. Statistics on Crystallographic Analysis

diffraction data	
space group	$P3_121$
cell parameters $a = b$, c (Å)	70.00, 70.00, 151.77
resolution (Å)	2.5
measured intensities	150 824
unique reflections	15 492
completeness (%)	99.9
R_{merge} (%)[a]	8.3 (30)
refinement	
R_{cryst} (%)[b]	20.3 (30.5)
reflections	14 555
protein atoms	3423
nucleotide atoms	99
solvent atoms	108
average B (Å^2)	22
geometry[c]	
bond distances (Å)	0.012
bond angle (deg)	1.9
torsion angle (deg)	2.0

[a] $R_{merge} = \sum_{hi} |I(h)_i - \langle I(h)\rangle| / \sum_{hi} I(h)_i$. The value in parentheses is for the 2.59−2.5 Å shell. [b] $R_{cryst} = \sum_h ||F_o| - |F_c|| / \sum_h |F_o|$ was calculated with X-PLOR on all reflections with $F > 2\sigma$. The value of R_{free} calculated on 7.5% randomly selected reflections is in parentheses. [c] Root-mean-square deviation from ideal values.

NDPK mutant H122G, in which the nucleophilic histidine was replaced by glycine. Addition of Im to reaction mixtures containing Mg·ATP and H122G resulted in the formation of an ImP product (Figure 2A). The first-order disappearance of ATP, as quantitated from the gel depicted in Figure 2A, is shown in Figure 2B; these data are representative of data used to obtain the rate constants described below. The first examples of chemical rescue of enzyme mutants were the functional substitution of a histidine by substrates containing histidine in subtilisin (*26*) and the functional substitution of a lysine by exogenously added amines in aspartate aminotransferase (*27*). Subsequently, several examples of rescue of histidine mutations by added Im have been reported (*28*−*34*), including the rescue of hexose-1-phosphate uridylyltransferase, which also has a nucleophilic histidine (*35*, *36*).

The importance of the covalent bond between histidine and NDPK was probed by comparing the second-order rate constant for reaction of ATP and wild-type NDPK with that of ATP and H122G·Im [$(k_{cat}/K_M)^{ATP}_{wt}$ and $(k_{cat}/K_M)^{ATP}_{Im}$; Scheme 2]. It was necessary to demonstrate saturation of H122G with Im to make this comparison. However, at the highest Im concentrations a modest downward curvature was observed in the Im dependence of the H122G reaction with ATP (Figure 3A). This curvature suggests binding of a second Im that is inhibitory, in addition to the Im that binds and rescues in the nucleophile site. Im and nucleotide bases

Table 2. Second-Order Rate Constants for Reactions of NDPK and H122G[a]

	$(k_{cat}/K_M)^{ATP}$		$(k_{cat}/K_M)^{ATP\gamma S}$		
	in M^{-1} s^{-1}	relative	in M^{-1} s^{-1}	relative	thio effect[b]
NDPK	2×10^6	2000	7×10^3	200	300
H122G·Im	4×10^4	40	4×10^3	100	10
H122G·H_2O	1×10^3	(1)	3×10^1	(1)	30

[a] 25 °C, 50 mM potassium EPPS, pH 7.8, 5 mM $MgCl_2$, $I = 0.3$ M (KCl); the second-order rate constants are defined in Scheme 2. [b] Thio effect $= (k_{cat}/K_M)^{ATP}/(k_{cat}/K_M)^{ATP\gamma S}$.

are structurally similar, and NDPK has little base specificity, so we considered the possibility that the inhibitory Im binds in the base site and competes with ATP binding. We tested this model by investigating the effect of Im on the wild-type reaction, in which the binding site for the nucleophilic Im is absent due to occupancy of the site by the active site histidine. This should allow unmasking of an inhibitory Im site. Indeed, Im inhibited the wild-type reaction with an inhibition constant of 0.45 M (Figure 3B). An inhibitory Im would be expected to bind similarly to both wild-type NDPK and H122G, so a binding constant of 0.45 M was assigned to the inhibitory H122G site on the basis of the Im inhibition of wild-type NDPK. This expectation is supported by the strong structural similarities between the nucleotide binding sites of wild-type NDPK and the H122G mutant, as described below, and by the observation that the binding affinity of AMP for H122G is within 2-fold of its binding affinity for wild-type NDPK (data not shown).

The saturation data for the mutant were therefore fit to a model with two Im, one that serves as the nucleophile and one, with a $K_i = 0.45$ M, that is responsible for the inhibition, as diagrammed in Figure 3C.[3] The data fit well to this model, with $K_d = 0.25$ M for binding of Im to the nucleophile site and $(k_{cat}/K_M)^{ATP}_{Im} = 4 \times 10^4$ M^{-1} s^{-1} for the reaction of H122G·Im with ATP (Figure 3A; Table 2). This rate constant is 50-fold less than the value of $(k_{cat}/K_M)^{ATP}_{wt}$ measured for the reaction of wild-type NDPK with ATP (Table 2).

[3] A random binding model is presented, although the data do not allow it to be distinguished from an ordered binding model for ATP and Im. One might expect that the H122G reaction follows an ordered mechanism, with Im binding first and ATP binding second, because Im may not be able to access the nucleophile cavity after ATP binds. However, because transfer of the phosphoryl group is slow relative to binding steps, all of the enzyme·substrate complexes depicted reach equilibrium concentrations; the kinetic measurements therefore do not distinguish between these binding models. The ordered binding model is a special case of the random binding model that is presented. Thus, the conclusions drawn herein hold whether or not binding is ordered.

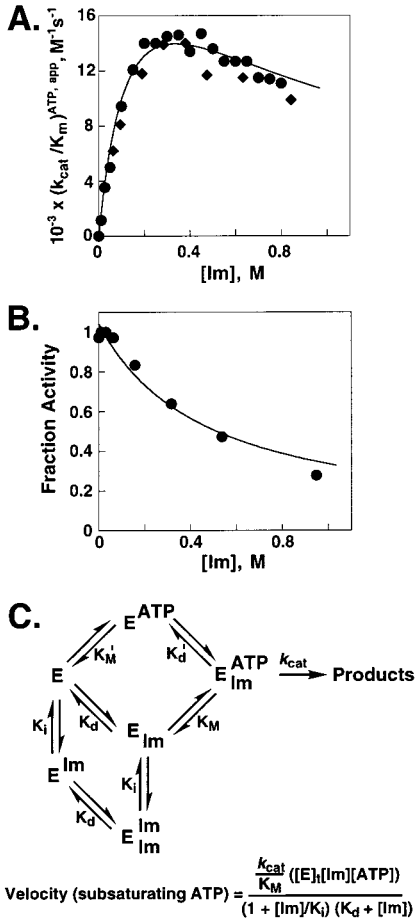

FIGURE 3: Evaluation of Im binding and saturation. (A) Im dependence of H122G rescue. Different symbols represent data from independent experiments. Data are fit to the two-Im model shown in panel C, with K_i for the inhibitory Im set to 0.45 M as described in the Results; $K_d = 0.25$ M for the functional Im and $(k_{cat}/K_M)_{Im}^{ATP} = 4 \times 10^4$ M^{-1} s^{-1} are obtained. The data in the plot do not reach this $(k_{cat}/K_M)_{Im}^{ATP}$ plateau because the rate increase corresponding to saturation of the nucleophilic Im is masked by inhibition from the second site Im, which also results in the downward curvature at high Im concentrations. (B) Im inhibition of wild-type NDPK $(k_{cat}/K_M)_{wt}^{ATP}$ activity was normalized by dividing the observed rate constant in the presence of inhibitor by the rate constant in the absence of inhibitor. The line is a nonlinear least-squares fit to competitive inhibition of NDPK activity and gives $K_i = 0.45$ M for Im. (C) Model for two site binding of Im to H122G (represented as E for clarity). The velocity equation shown below the model is a simplified version of the general velocity equation for this model that holds when ATP is subsaturating, as was the case for all experiments reported herein.

It is possible that $(k_{cat}/K_M)_{Im}^{ATP}$ for the mutant reaction is underestimated by up to 3-fold due to the assumption that the Im inhibition constants for wild-type NDPK and H122G are identical. This is because the same curve shape would be observed regardless of whether the nucleophilic Im (described by K_d) or the inhibitory Im (described by K_i) has the greater affinity for H122G in the model of Figure 3C. An attempt was made to deconvolute the two H122G Im binding sites by measuring the binding constant for Im in the presence of saturating ATP (K_d'). Because the inhibitory Im directly competes with ATP for binding, these conditions were expected to raise the apparent Im inhibition constant while leaving the binding constant for the nucleophilic Im unchanged. However, this experiment was complicated by the finding that binding of ATP also weakens the binding

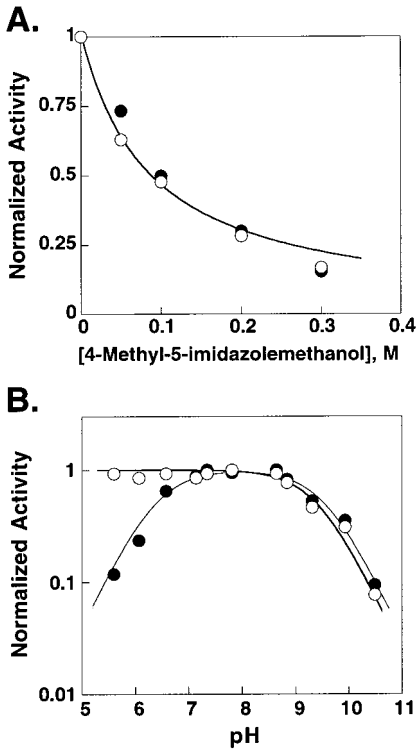

FIGURE 4: H122G catalyzes the hydrolysis of ATP. (A) Identical inhibition of the hydrolysis (○) and Im (●) reactions of H122G by 4-methyl-5-imidazolemethanol. For comparison, activity was normalized by dividing the observed rate constant in the presence of inhibitor by the rate constant in the absence of inhibitor. The line is a nonlinear least-squares fit to the combined data for competitive inhibition of both activities by 4-methyl-5-imidazolemethanol and gives $K_i = 80$ mM. (B) The pH dependencies of the hydrolysis (○) and Im (●) reactions of H122G. For comparison, activity was normalized by dividing the observed rate constant at a given pH by the maximal rate constant for that activity. The lines are nonlinear least-squares fits to one and two ionizations for the hydrolysis and Im reactions, respectively. The fits give a pK_a value of 9.5 ± 0.1 for the hydrolysis reaction and pK_a values of 6.5 ± 0.1 and 9.5 ± 0.1 for the Im reaction.

of the nucleophilic Im, such that saturating Im concentrations could not be achieved when the enzyme was saturated with ATP (i.e., $K_d' > K_d$; data not shown). Although this uncertainty in $(k_{cat}/K_M)_{Im}^{ATP}$ for the H122G·Im reaction could not be resolved, it does not affect the conclusions.

Chemical Rescue of H122G by Water. Reaction mixtures containing Im, Mg·ATP, and H122G produced P_i in addition to ImP (Figure 2A). P_i was also observed in reaction mixtures containing Mg·ATP and H122G in the absence of Im (Figure 2C). To determine whether P_i arose from a contaminating ATPase activity or from the attack of water upon ATP in the H122G active site, we investigated the inhibition of ImP and P_i formation by 4-methyl-5-imidazolemethanol. 4-Methyl-5-imidazolemethanol is an analogue of Im that binds to H122G but does not react. Figure 4A shows that both activities were inhibited by 4-methyl-5-imidazolemethanol with the same inhibition constant ($K_i = 80$ mM), suggesting that both reactions occur in the same active site. The pH dependencies of the two reactions provided further evidence that the hydrolysis and Im reactions share a common H122G active site (Figure 4B). Both reactions exhibit a pK_a of 9.5 and share a common plateau between pH 9 and 7. As expected, the pH dependencies diverge below pH 7, with a best fit to a pK_a of 6.5 for the Im reaction that is consistent

with protonation of free Im, a pK_a that is not shared by the water nucleophile.

Assignment of the ATP hydrolysis reaction to the H122G active site allowed the determination of $(k_{cat}/K_M)^{ATP}_{H_2O}$ for this reaction (Scheme 2). The second-order rate constant for ATP hydrolysis of 1×10^3 M^{-1} s^{-1} is 40-fold smaller than $(k_{cat}/K_M)^{ATP}_{Im}$ measured for H122G·Im and 2×10^3-fold smaller than $(k_{cat}/K_M)^{ATP}_{wt}$ measured for wild-type NDPK (Table 2).

Thio Effects for Wild-Type and H122G Reactions. ATPγS was substituted for ATP as substrate for the wild-type NDPK reaction and for the reactions of H122G with Im and water, and $(k_{cat}/K_M)^{ATP\gamma S}$ values were obtained (Table 2). The thio effect of 300 for the wild-type reaction exceeded the thio effects of 10 and 30 observed for the H122G·Im and H122G·H_2O reactions, respectively.

Reactions of Amines with ATP and H122G. The addition of primary amines to reaction mixtures containing Mg·ATP and H122G resulted in the production of the corresponding amine phosphate products. Ion-exchange HPLC was used to separate amine phosphate and P_i products generated from competing nucleophilic attack on ATP by amines and water, respectively, so that partitioning between reaction with the amine and reaction with water could be followed. This allowed the rate constant for the reaction of the amine relative to that for reaction of water, k_{rel}, to be determined (Scheme 3).[4]

The relative rate constants in Table 3 were calculated from the fraction of amine phosphate formed and the molar concentrations of nucleophilic amine ($[RNH_2]$) and water present, according to the equation in Scheme 3. A plot of amine pK_a versus log k_{rel} gives a slope of $\beta_{nucleophile} = 0.16 \pm 0.06$ (Figure 5). Caveats to the use and interpretation of LFERs on enzymes in general and for H122G in particular are considered in the Discussion.

The Structure of the H122G·ADP·P_i Complex. The structure of the H122G protein in crystals grown in the presence of ATP is very similar to wild-type NDPK structures, and especially to the complex with the transition state analogue ADP·AlF_3 (*24*), which crystallizes in the same space group and is therefore used for comparison (Figure 6). The electron density at the nucleotide binding site of H122G demonstrates the presence of ADP and P_i rather than ATP, presumably due to hydrolysis of ATP by H122G during crystallization (Figure 6A). The root-mean-square distance between equivalent C_α atoms in the H122G and wild-type structures is 0.38 Å, comparable to the estimated error in the atomic coordinates (0.28 Å from a Luzzati plot). Thus, the mutant protein has the same quaternary (hexameric) and tertiary structure as the wild-type. Locally, the mutation has little effect beyond the deletion of the histidine side chain: the C_α position of residue 122, the position of mutation, moves by less than 0.5 Å, and the main-chain conformation of adjacent residues in strand β4 is unchanged (Figure 6B). In the wild-type protein, the carboxylate of Glu 133 receives a hydrogen bond from His 122, helping to orient the Im group. Remarkably, the Glu 133 side chain retains its position and conformation in the absence of His 122. Another interaction of the carboxylate with the hydroxyl of Ser 124 presumably maintains it in place in the mutant and wild-type structures. The nucleophile binding pocket is therefore retained in the H122G mutant (Figure 6C), allowing exogenous Im to bind to H122G and rescue its reaction with ATP.

The conformation of ADP is the same as in the ADP·AlF_3 complex, and the characteristic hydrogen bond between the 3′-hydroxyl of the ribose and the O_7 oxygen of the

Table 3. Relative Rate Constants for H122G-Catalyzed Reactions of Amines and ATP^{4-}·Mg^{2+} [a]

RNH_2	pK_a [b]	k_{rel}
$CH_3CH_2CH_2CH_2NH_2$	10.6	8.1 ± 2.1
$CH_3CH_2CH_2NH_2$	10.6	4.7 ± 1.7
$CH_3CH_2NH_2$	10.6	1.1 ± 0.1
CH_3NH_2	10.6	3.9 ± 1.6
$NH_2CH_2CH_2NH_2$	10.0	0.9 ± 0.3 [c]
$HOCH_2CH_2NH_2$	9.5	4.6 ± 2.4
$H_2C{=}CHCH_2NH_2$	9.5	4.7 ± 1.0
HNH_2	9.3	2.9 ± 0.4
$CH_3OCH_2CH_2NH_2$	9.2	1.3 ± 0.3
$CBrH_2CH_2CH_2NH_2$	8.9	4.3 ± 1.5
$CClH_2CH_2CH_2NH_2$	8.9 [d]	4.5 ± 0.7
$CBrH_2CH_2NH_2$	8.5	5.2 ± 2.4
$CClH_2CH_2NH_2$	8.5 [d]	1.1 ± 0.1
$CFH_2CH_2NH_2$	8.5 [d]	0.7 ± 0.3
$HC{\equiv}CCH_2NH_2$	8.2	2.9 ± 0.6
$HONH_2$	6.0	31 ± 3.0
$CF_3CH_2NH_2$	5.7	0.06 ± 0.02
$N{\equiv}CCH_2NH_2$	5.3	0.5 ± 0.2
CH_3ONH_2	4.6	2.0 ± 0.7

[a] 25 °C, 5 mM $MgCl_2$, I = 0.3 M (KCl). [b] From ref *54* unless otherwise noted. [c] Statistically corrected for the presence of two amine groups. [d] The pK_a of chloropropylamine was assumed to be the same as that of bromopropylamine, and the pK_a values of chloro- and fluoroethylamine were assumed to be identical to that of bromoethylamine; chloro, fluoro, and bromo substituents are similarly electron-withdrawing, resulting in similar ionization constants for compounds that are halogenated at identical positions. For example, chloro, fluoro, and bromo substituents at the meta position of aniline result in pK_a values of 3.3, 3.5, and 3.4 (*54*). Different pK_a values for chloropropylamine, chloroethylamine, and fluoroethylamine would not alter the conclusions drawn in the text.

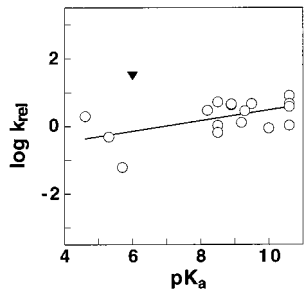

FIGURE 5: Dependence of H122G-catalyzed phosphoryl transfer from ATP on the pK_a of the amine nucleophile. The data are from Table 3. The line is a least-squares fit to the data and gives a slope of $\beta_{nucleophile} = 0.16 \pm 0.06$. The reaction of hydroxylamine (▼) is omitted from the fit because of a potential α-effect (*58*); inclusion gives $\beta_{nucleophile} = 0.09 \pm 0.07$.

[4] The amine phosphate product of the partitioning reaction shown in Scheme 3 is depicted in its deprotonated form. Although the protonation state of an amine phosphate in a given experiment depends on the pK_a of this product and the pH of the reaction, the proton is expected to be present in the rate-limiting transition state for reactions with limited bond formation to the incoming nucleophile (*4*). It is not known if the proton is lost while the product is at the active site or if the product first diffuses away, but this would not affect the conclusions herein, as these events are expected to occur after the rate-limiting step. For simplicity, third-order reactions of amines or H_2O with H122G and ATP are compared in Scheme 3, resulting in k_{rel} values that are unitless. Because k_{rel} is used to compare the amines with one another, the choice of standard state for the water reaction affects all of the k_{rel} values equivalently and therefore does not affect this comparison.

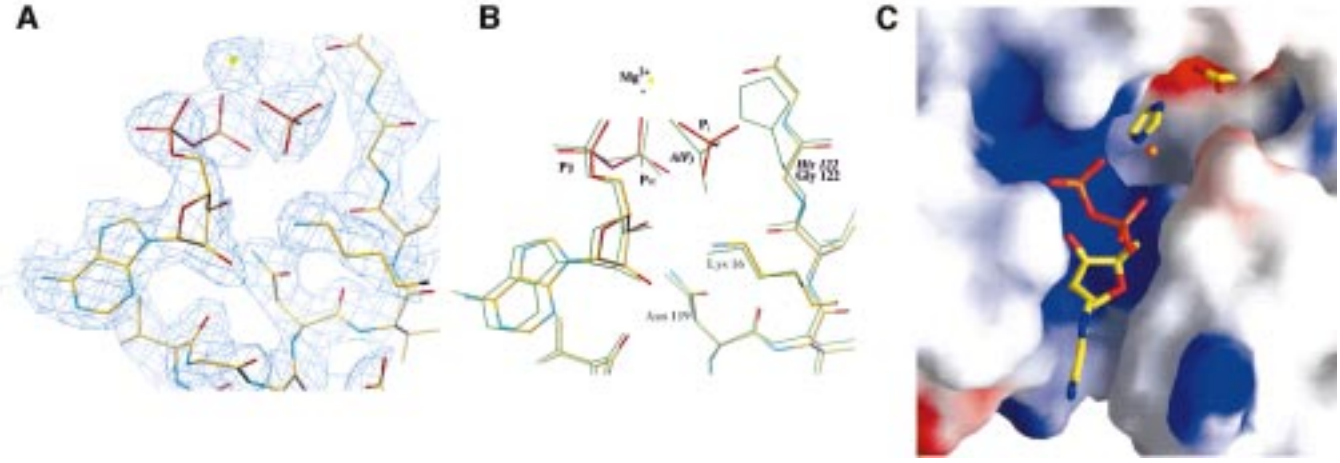

FIGURE 6: The H122G active site. (A) The $2F_o - F_c$ electron density map phased with the final model and contoured at 1σ. ADP and P_i, products of ATP hydrolysis, are bound to H122G and ligated by Mg^{2+} (yellow sphere, top center). (B) Superposition of the H122G structure (colored by atom type) with wild-type NDPK in complex with Mg·ADP and AlF_3 (green bonds). In the H122G structure, P_i replaces the AlF_3 moiety located between the β-phosphate of ADP and the His 122 side chain. The absence of a side chain at residue 122 in the H122G structure leaves room for P_i. C_α atoms of the respective structures were used to produce this superposition. (C) Model of the H122G active site and nucleophile binding pocket. The protein, nucleotide, and Mg^{2+} (orange sphere) are from the H122G structure, and the Im is taken from the His 122 side chain of wild-type NDPK after superposition with H122G. The Im is located in a cavity between the β-phosphate of ADP and the side chain of Glu 133 (top right). The protein surface is colored according to electrostatic potential (positive blue, negative red). The orientation has been rotated by ~90° relative to panels A and B. For clarity, the side chains of His 55 and Asp 125, which are in front of the Im site in this view, have been deleted. Created with GRASP (*59*).

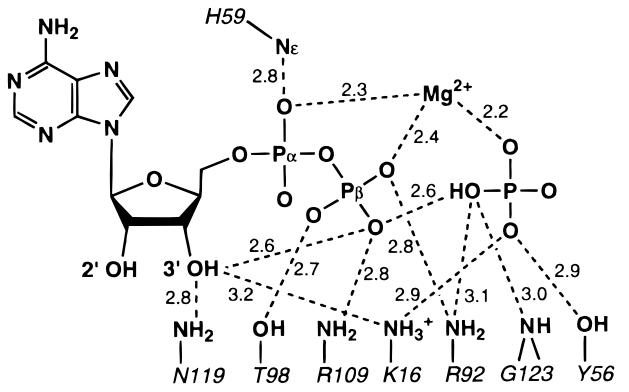

FIGURE 7: Polar interactions of ADP and P_i bound to H122G. Residue numbers are italicized. Distances (in Å) are averaged over the three subunits present in the asymmetric unit. The standard deviation from this average is 0.13 Å.

β-phosphate is retained. Relative to its position in the ADP·AlF_3 complex, the nucleotide has undergone a small (~0.3 Å) rigid-body shift toward the inside of the protein, but all interactions with protein groups are maintained (Figure 7). P_i approximately occupies the position of the AlF_3 group and makes similar interactions. Mg^{2+} ligates P_i in addition to the two phosphates of ADP. The P_i is shifted by about 0.8 Å toward residue 122, relative to the AlF_3 in the wild-type structure; this shift is made possible by the absence of the side chain. Protein groups that interact with P_i follow its movement: the amino group of Lys 16 moves by 0.7 Å, and the guanidinium group of Arg 92 rotates and moves by 1.0 Å.

DISCUSSION

Importance of the Nucleophile for Catalysis. The second-order rate constant for the reaction of wild-type NDPK and ATP is 50-fold greater than the corresponding rate constant for the reaction of H122G·Im and ATP (Table 2), indicating that a covalent linkage between enzyme and nucleophile provides a 50-fold catalytic advantage in this system. A noncovalent binding site for the nucleophile may also contribute to catalysis. H122G·Im, with the canonical nucleophile bound, reacts toward ATP with a 40-fold greater rate constant than does H122G·H_2O, with an adventitious nucleophile bound (Table 2), whereas nonenzymatically Im is ~10-fold more reactive toward ATP than is water (S.J.A. and D.H., manuscript in preparation). This comparison suggests that there is a catalytic advantage of ~4-fold from the specific nucleophile binding site. Together, these results suggest that the covalent linkage and binding site for the nucleophile provide an overall contribution of $\sim 10^2$ to catalysis.

This 10^2-fold effect could arise because the enzyme benefits from aligning the nucleophile with respect to the substrate and with respect to other catalytic groups. This entropic activation of the nucleophile would be accomplished, at least in part, by a covalent linkage and a binding site for the nucleophile, with catalysis suffering when these positioning interactions are removed in the H122G reaction. An alternative model for the 10^2-fold effect is that H122G has a structurally perturbed active site. If this were the case, the 10^2-fold disadvantage of the mutant reaction could reflect a requirement for a conformational rearrangement prior to reaction or a compromised reaction from an alternative conformation. Although the possibility that very small perturbations within the active site are responsible for the deleterious effects on catalysis cannot be eliminated, the X-ray structure of H122G in complex with ADP·P_i indicates that deletion of the His 122 side chain does not substantially perturb the three-dimensional structure, even locally, and that the mutant binds Mg·ADP similarly to wild-type (Figure 6). In addition, the binding affinity of AMP for H122G is within 2-fold of its binding affinity for wild-type NDPK (data not shown), providing no indication of a disordered active site.

Nucleophilic Activation by Positioning in the NDPK Active Site. The 10^2-fold catalytic effect of a positioned nucleophile

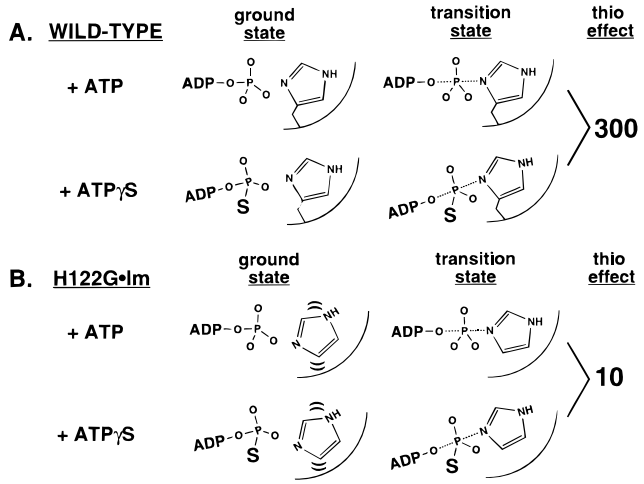

FIGURE 8: Positioning model for different thio effects observed for wild-type NDPK and H122G. Reactions of ATP and ATPγS with wild-type (A) or H122G·Im (B) are depicted schematically. Charges are not shown for simplicity. (A) A thio effect of 300 is observed for the wild-type reaction because the bulky sulfur substituent of ATPγS disrupts positioning between nucleophile and substrate. (B) A smaller thio effect of 10 is observed for the H122G reaction. Alignment is already disrupted because of the absence of a covalent bond to the nucleophile, depicted by motion lines around Im, so the ATPγS substitution is less deleterious to positioning.

can be explained by participation of the nucleophile in a network of active site interactions that form a template for the transition state. In solution there is an entropic barrier to aligning substrates with respect to each other and with respect to any chemical catalysts that may be present. However, an enzyme can reduce this entropic barrier by preorganizing a reaction template in which catalytic groups and substrates are optimally positioned (*12*). This template is maintained by alignment of components relative to one another, such that disruption of one component of the network can disrupt precise positioning within the active site.

Results with the alternative substrate ATPγS provide further evidence for catalysis from positioning of the nucleophile and transferred phosphoryl group within a network of active site interactions (Table 2). Disruption of the positioning of either the nucleophile, by breaking the covalent connection to the amide backbone, or ATP, by introduction of a thio substituent at the γ-phosphoryl group, is deleterious to catalysis (Figure 8). However, making the second disruption gives a much smaller effect, as depicted schematically in the model of Figure 8. For example, for the wild-type enzyme the replacement of ATP with ATPγS results in a 300-fold decrease in the rate constant, whereas the analogous switch from ATP to ATPγS gives a thio effect of only 10 when the covalent attachment to the nucleophile is broken in the H122G·Im complex. The bulky sulfur substituent of ATPγS presumably disrupts positioning between the nucleophile and substrate in the wild-type active site, resulting in the large thio effect. In H122G·Im precise alignment is already disrupted because of the absence of a covalent bond to the nucleophile, so that the ATPγS substitution has a smaller effect on catalysis (Figure 8).

The picture of the wild-type NDPK active site that is provided by the crystal structure of the enzyme with the transition state analogue ADP·AlF_3 bound is also consistent with precise positioning of the nucleophile and transferred phosphoryl group within a network of active site interactions (*24*). There are no covalent bonds to the AlF_3 moiety, which represents the transferred phosphoryl group in this structure, yet it is aligned with both the nitrogen of the His 122 nucleophile and the $\beta-\gamma$ bridging oxygen of the ADP leaving group, as expected for an in-line displacement. The enzyme's ability to enforce this alignment even in the absence of a covalent bond to the phosphoryl group analogue attests to the presence of a network of positioning interactions (for related examples, see refs *37*−*40*).

In a double displacement reaction related to that of NDPK, hexose-1-phosphate uridylyltransferase catalyzes the interconversion of UDP-galactose and glucose-1-phosphate with UDP-glucose and galactose-1-phosphate via a covalent intermediate. Its nucleophilic histidine attacks a UDP-sugar to produce a uridylylated histidine enzyme and a sugar phosphate; this enzyme intermediate is subsequently attacked by another sugar phosphate to complete the interconversion. Frey and co-workers replaced the histidine nucleophile with glycine in this system (H166G), and Im rescued the mutant enzyme for reaction with UDP-glucose (*35*, *41*). Comparison of the rate constant $(k_{cat}/K_M)^{UDP-glucose}$ for wild-type and Im-rescued H166G uridylyltransferases [analogous to $(k_{cat}/K_M)^{ATP}$ for NDPK and H122G·Im; Scheme 2] revealed a 130-fold advantage for the covalently attached nucleophile. This apparent entropic advantage for uridylyltransferase is similar to the 50-fold advantage from a covalent nucleophile for NDPK, despite the expectation from nonenzymatic studies that the phosphodiester-like reaction of uridylyltransferase proceeds through a more associative transition state than does the phosphomonoester-like reaction of NDPK (*1*, *2*).

The Small Observed $\beta_{nucleophile}$ Is Consistent with a Dissociative Transition State. Amine nucleophiles of disparate pK_a react similarly toward ATP in the H122G reaction (Table 3, Figure 5). The simplest interpretation of this observation, illustrated by the shallow $\beta_{nucleophile}$ slope of Figure 5, is that the transition state for the reaction of H122G and amines is dissociative, with little bond formation to the nucleophile. The $\beta_{nucleophile}$ value of 0.16 ± 0.06 is similar to previously measured $\beta_{nucleophile}$ values of 0.14 ± 0.04 for dephosphorylation of a protein tyrosine phosphatase by alcohols (*42*) and 0.07 ± 0.08 for peptide phosphorylation by a protein tyrosine kinase (*10*). However, this correlation must be interpreted with caution because of pitfalls associated with enzymatic LFERs (*43*, *44*).

A LFER must monitor the chemical step of the reaction under investigation to report on the chemical transition state. The k_{rel} values measured for H122G-catalyzed reactions of primary amines and ATP are small in comparison to the corresponding k_{rel} for the Im reaction ($k_{rel} = 6 \times 10^3$ for Im, calculated using Scheme 3), suggesting that no common slow step limits these reactions and that phosphoryl transfer is rate-limiting for the primary amines. However, there is significant scatter in the LFER data set for the H122G reactions (Table 3, Figure 5). These deviations suggest that the H122G nucleophile binding pocket influences the reactivity of individual amines. However, it is not possible to resolve with confidence the steric, electrostatic, and solvation effects that each influence reactivity within this restricted pocket, nor would these factors be expected to affect a specified subset of the amine nucleophiles uniformly. We have therefore considered all of the amines together,

while recognizing that this LFER alone cannot firmly establish the nature of this transition state and that a transition state with increased associative character is not ruled out. Nevertheless, previous nonenzymatic and enzymatic studies (see Introduction) coupled with the observed shallow $\beta_{nucleophile}$ for the H122G-catalyzed reaction lead to a working model in which phosphoryl transfer at the NDPK active site follows a dissociative, metaphosphate-like transition state, similar to that observed in solution.

Nucleophilic Activation by Positioning in a Dissociative Transition State. Entropy loss is not expected to scale linearly with the degree of bond formation, so entropic activation of the nucleophile may be important even for reactions with substantially dissociative transition states.[2] Comparisons of model reactions suggested that an effective molarity of 10 M arises from positioning of a phosphorylated pyridine and acetate by Mg^{2+} in a dissociative phosphoryl transfer reaction (*45*, *46*); the effective molarity is the rate advantage, compared with a standard state of 1 M, from positioning of the reactants by Mg^{2+} in order to overcome the entropic barrier of the reaction (*15*). The amount of enzymatic catalysis that can be derived from entropic activation of a nucleophile in a dissociative transition state is not known, but analysis of activation parameters for nonenzymatic phosphoryl transfer suggests that there is a significant entropic barrier for these reactions (*47*). NPDK appears to catalyze phosphoryl transfer via a dissociative transition state and derives a 10^2-fold catalytic advantage from a positioned nucleophile. These results suggest that precise positioning of a nucleophile can be a significant contributor to enzymatic catalysis even when there is little bond formation to the nucleophile in the transition state.

Nucleophilic Activation Within the Context of Overall Catalysis by NDPK. Enzymes appear to catalyze reactions through multiple interactions that each provide a modest amount of transition state stabilization (*12*), and a positioned nucleophile in the context of a network of active site interactions is one component of the transition state stabilization conferred by NDPK. Comparison of the second-order rate constant for the nonenzymatic reaction of Im and ATP with the second-order rate constant for reaction of NDPK and ATP indicates that the enzymatic reaction is catalyzed 10^{15}-fold over background (S.J.A. and D.H., manuscript in preparation). Positioning of the nucleophile by a covalent bond and a binding pocket appears to provide a $\sim 10^2$-fold advantage. Nevertheless, H122G retains a 10^{13}-fold rate enhancement over the uncatalyzed reaction even in the hydrolysis reaction, in which it lacks a positioned nucleophile. Additional catalytic interactions appear to converge upon the nucleotide side of the active site; mutagenesis and structural studies have implicated several residues that interact with the nucleotide as catalytic (*18*, *48*). An intramolecular hydrogen bond between the 3′-OH and the $\beta-\gamma$ bridging oxygen of the nucleotide has also been proposed to be catalytic, as replacement of the 3′-OH of ATP with 3′−H to give 3′-dATP results in a 10^3-fold decrease in k_{cat}/K_M (*21*, *24*, *48*−*50*). This hydrogen bond would be expected to stabilize developing negative charge on the NDP leaving group in the transition state (*51*).

Conclusions and Implications. This work suggests that phosphoryl transfer enzymes are able to activate their nucleophiles for reaction by positioning them with respect to substrate and with respect to other enzyme functional groups. Entropy is lost even in transition states in which only a small amount of bond formation has occurred, and enzymatic reduction of this entropic barrier appears to provide significant catalysis. This raises the possibility that entropic activation of the nucleophile may also provide substantial catalysis for other biological reactions that exhibit only a small amount of bond formation to the nucleophile in the transition state. Candidate reactions include prenyl transfer through carbocation-like transition states and glycosyl transfer via oxocarbonium-like transition states (*52*, *53*).

More generally, enzyme interactions that have been assigned a role in chemical activation may additionally provide entropic activation. For example, groups suggested to act as general base catalysts in kinase and related reactions may help position the nucleophile with respect to the transferred phosphoryl group. Similarly, electrostatic interactions between phosphodiesterases and the developing charges on the transferred $P(OR)O_2^-$ group are often proposed to enhance the chemical reactivity of phosphodiester substrates. In some cases the electrostatic interactions may also or instead consolidate a positioned network of active site interactions, thereby stabilizing the transition state.

ACKNOWLEDGMENT

We are grateful to members of the Herschlag lab for comments on the manuscript.

REFERENCES

1. Benkovic, S. J., and Schray, K. J. (1978) in *Transition States of Biological Processes* (Gandour, R. D., Ed.) pp 493−527, Plenum, New York.
2. Thatcher, G. R. J., and Kluger, R. (1989) *Adv. Phys. Org. Chem. 25*, 99−265.
3. Hengge, A. C. (1998) in *Comprehensive Biological Catalysis: A Mechanistic Reference* (Sinnott, M., Ed.) Vol. 1, pp 517−542, Academic Press, San Diego, CA.
4. Jencks, W. P. (1972) *J. Am. Chem. Soc. 94*, 4731−4732.
5. Admiraal, S. J., and Herschlag, D. (1995) *Chem. Biol. 2*, 729−739.
6. Herschlag, D., and Jencks, W. P. (1987) *J. Am. Chem. Soc. 109*, 4665−4674.
7. Herschlag, D., and Jencks, W. P. (1989) *J. Am. Chem. Soc. 111*, 7587−7596.
8. Jencks, W. P. (1985) *Chem. Rev. 85*, 511−527.
9. Cleland, W. W., and Hengge, A. C. (1995) *FASEB J. 9*, 1585−1594.
10. Kim, K., and Cole, P. A. (1997) *J. Am. Chem. Soc. 119*, 11096−11097.
11. Kim, K., and Cole, P. A. (1998) *J. Am. Chem. Soc. 120*, 6851−6858.
12. Jencks, W. P. (1975) *Adv. Enzymol. 43*, 219−410.
13. Kirby, A. J. (1980) *Adv. Phys. Org. Chem. 17*, 183−278.
14. Page, M. I., and Jencks, W. P. (1971) *Proc. Natl. Acad. Sci. U.S.A. 68*, 1678−1683.
15. Page, M. I. (1973) *Chem. Soc. Rev. 2*, 295−323.
16. Kunkel, T. A. (1985) *Proc. Natl. Acad. Sci. U.S.A. 82*, 488−492.
17. Lacombe, M.-L., Wallet, V., Troll, H., and Véron, M. (1990) *J. Biol. Chem. 265*, 10012−10018.
18. Tepper, A., Dammann, H., Bominaar, A. A., and Véron, M. (1994) *J. Biol. Chem. 269*, 32175−32180.
19. Gill, S. C., and Von Hippel, P. H. (1989) *Anal. Biochem. 182*, 319−326.
20. Lascu, I., Deville-Bonne, D., Glaser, P., and Véron, M. (1993) *J. Biol. Chem. 268*, 20268−20275.

21. Bourdais, J., Biondi, R., Sarfati, S., Guerreiro, C., Lascu, I., Janin, J., and Véron, M. (1996) *J. Biol. Chem. 271*, 7887−7890.
22. Otwinowski, Z., and Minor, W. (1997) *Methods Enzymol. 276*, 307−326.
23. CCP4. Collaborative Computational Project, No. 4. (1994) *Acta Crystallogr., Sect. A 50*, 157−163.
24. Xu, Y.-W., Moréra, S., Janin, J., and Cherfils, J. (1997) *Proc. Natl. Acad. Sci. U.S.A. 94*, 3579−3583.
25. Brünger, A. T., Kuriyan, J., and Karplus, M. (1987) *Science 235*, 458−460.
26. Carter, P., and Wells, J. A. (1987) *Science 237*, 394−399.
27. Toney, M. D., and Kirsch, J. F. (1989) *Science 243*, 1485−1488.
28. Barrick, D. (1994) *Biochemistry 33*, 6546−6554.
29. Barrick, D., Ho, N. T., Simplaceanu, V., Dahlquist, F. W., and Ho, C. (1997) *Nat. Struct. Biol. 4*, 78−83.
30. Carter, P., Abrahmsen, L., and Wells, J. A. (1991) *Biochemistry 30*, 6142−6148.
31. Huang, S., and Tu, S.-C. (1997) *Biochemistry 36*, 14609−14615.
32. Newmyer, S. L., and Ortiz de Montellano, P. R. (1996) *J. Biol. Chem. 271*, 14891−14896.
33. Newmyer, S. L., Sun, J., Loehr, T. M., and Ortiz de Montellano, P. R. (1996) *Biochemistry 35*, 12788−12795.
34. Tu, C., Silverman, D. N., Forsman, C., Jonsson, B.-H., and Lindskog, S. (1989) *Biochemistry 28*, 7913−7918.
35. Kim, H., Ruzicka, F., and Frey, P. A. (1990) *Biochemistry 29*, 10590−10593.
36. Ruzicka, F. J., Geeganage, S., and Frey, P. A. (1998) *Biochemistry 37*, 11385−11392.
37. Nassar, N., Hoffman, G. R., Manor, D., Clardy, J. C., and Cerione, R. A. (1998) *Nat. Struct. Biol. 5*, 1047−1052.
38. Zhou, G., Somasundaram, T., Blanc, E., Parthasarathy, G., Ellington, W. R., and Chapman, M. S. (1998) *Proc. Natl. Acad. Sci. U.S.A. 95*, 8449−8454.
39. Scheffzek, K., Ahmadian, M. R., Kabsch, W., Wiesmüller, L., Lautwein, A., Schmitz, F., and Wittinghofer, A. (1997) *Science 277*, 333−338.
40. Schlichting, I., and Reinstein, J. (1997) *Biochemistry 36*, 9290−9296.
41. Thoden, J. B., Ruzicka, F. J., Frey, P. A., Rayment, I., and Holden, H. M. (1997) *Biochemistry 36*, 1212−1222.
42. Zhao, Y., and Zhang, Z.-Y. (1996) *Biochemistry 35*, 11797−11804.
43. Kirsch, J. F. (1972) in *Advances in Linear Free Energy Relationships* (Chapman, N. B., and Shorter, J., Eds.) pp 369−400, Plenum, New York.
44. Hollfelder, F., and Herschlag, D. (1995) *Biochemistry 34*, 12255−12264.
45. Herschlag, D., and Jencks, W. P. (1990) *Biochemistry 29*, 5172−5179.
46. Herschlag, D., and Jencks, W. P. (1990) *J. Am. Chem. Soc. 112*, 1942−1950.
47. Hoff, R. H., and Hengge, A. C. (1998) *J. Org. Chem. 63*, 6680−6688.
48. Moréra, S., Chiadmi, M., LeBras, G., Lascu, I., and Janin, J. (1995) *Biochemistry 34*, 11062−11070.
49. Cherfils, J., Moréra, S., Lascu, I., Véron, M., and Janin, J. (1994) *Biochemistry 33*, 9062−9069.
50. Schneider, B., Xu, Y. W., Sellam, O., Sarfati, R., Janin, J., Véron, M., and Deville-Bonne, D. (1998) *J. Biol. Chem. 273*, 11491−11497.
51. Maegley, K. A., Admiraal, S. J., and Herschlag, D. (1996) *Proc. Natl. Acad. Sci. U.S.A. 93*, 8160−8166.
52. Gibbs, R. A. (1998) in *Comprehensive Biological Catalysis: A Mechanistic Reference* (Sinnott, M., Ed.) Vol. 1, pp 31−118, Academic Press, San Diego, CA.
53. Davies, G., Sinnott, M. L., and Withers, S. G. (1998) in *Comprehensive Biological Catalysis: A Mechanistic Reference* (Sinnott, M., Ed.) Vol. 1, pp 119−209, Academic Press, San Diego, CA.
54. Jencks, W. P., and Regenstein, J. (1976) in *Handbook of Biochemistry and Molecular Biology* (Fasman, G. D., Ed.) pp 305−351, CRC Press, Cleveland, OH.
55. Hengge, A. C., Edens, W. A., and Elsing, H. (1994) *J. Am. Chem. Soc. 116*, 5045−5049.
56. Horn, H., and Ahlrichs, R. (1990) *J. Am. Chem. Soc. 112*, 2121−2124.
57. Rajca, A., Rice, J. E., Streitwieser, A., Jr., and Schaefer, H. F., III (1987) *J. Am. Chem. Soc. 109*, 4189−4192.
58. Jencks, W. P. (1987) in *Catalysis in Chemistry and Enzymology*, pp 107−111, Dover, New York.
59. Nicholls, A., Sharp, K., and Honig, B. (1992) *Proteins 11*, 281−296.

BI9827565